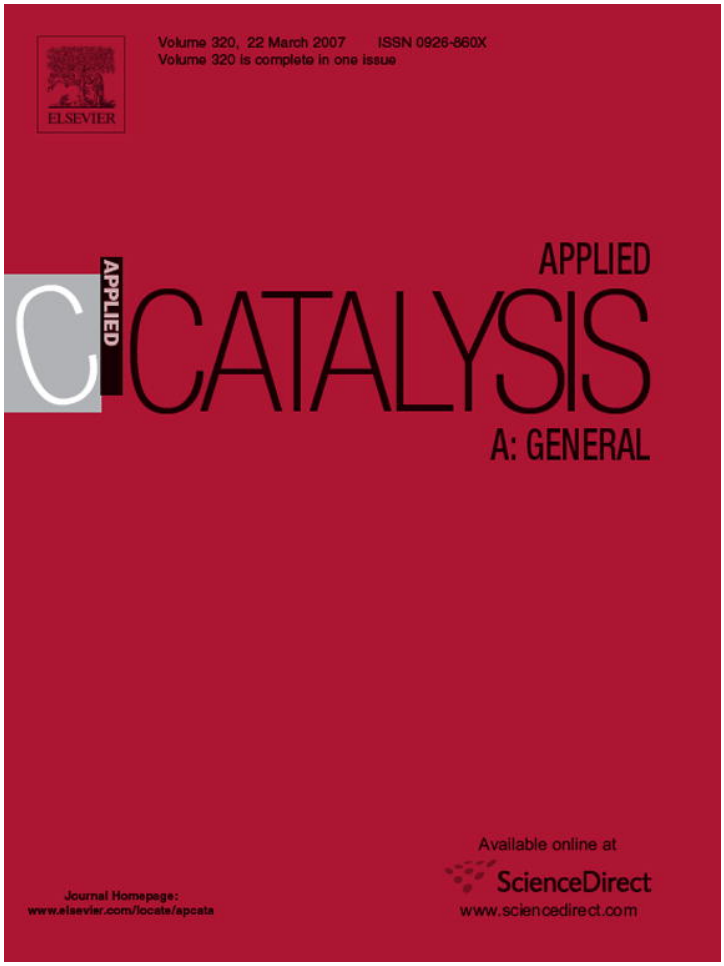

Available online at www.sciencedirect.com
ScienceDirect
Applied Catalysis A: General 320 (2007) 134–143
APPLIED CATALYSIS A: GENERAL
www.elsevier.com/locate/apcata

Influence of silica calcination temperature on the performance of supported catalyst SiO_2–^{n}BuSnCl$_3$/MAO/(^{n}BuCp)$_2$ZrCl$_2$ polymerizing ethylene without separately feeding the MAO cocatalyst

M. Atiqullah [a,*], M.N. Akhtar [a], A.A. Moman [b], A.H. Abu-Raqabah [b], S.J. Palackal [b], H.A. Al-Muallem [c], O.M. Hamed [b]

[a] *Center for Refining & Petrochemicals, Research Institute, King Fahd University of Petroleum & Minerals, Dhahran 31261, Saudi Arabia*
[b] *Saudi Basic Industries Corporation (SABIC), R&T Center, P.O. Box 42503, Riyadh 11551, Saudi Arabia*
[c] *Department of Chemistry, King Fahd University of Petroleum & Minerals, Saudi Arabia*

Received 15 October 2006; received in revised form 9 January 2007; accepted 10 January 2007
Available online 18 January 2007

Abstract

The effects of support calcination temperature, an important catalyst synthesis parameter, on the overall performance of the supported catalyst [silica ES70–^{n}BuSnCl$_3$/MAO/(^{n}BuCp)$_2$ZrCl$_2$], polymerizing ethylene without separately feeding the MAO cocatalyst, were studied. The silica was calcined at 250, 450, 600, and 800 °C for 4 h. ^{n}BuSnCl$_3$ was used to functionalize the silica.

Ethylene was polymerized using the synthesized catalysts at 8.5 bar(g) in hexane for 1 h. No reactor fouling was observed. Free-flowing polymer particles with bulk density (0.23–0.27 g/ml) and a fairly spherical morphology similar to that of the catalyst particles were obtained. Also, the particle size distribution of the polymer resembled that of the catalyst. Therefore, the replication phenomenon from catalyst to polymer took place. The narrow PSD span (1.41) indicates that the resulting polyethylenes are suitable for various mixing-intensive polymer applications. The MAO cocatalyst-free ethylene polymerization instantaneously formed a polymer film around the catalyst particle, which coated/immobilized the catalyst constituents; this is how leaching was in situ prevented which favored heterogeneous catalysis to occur. The catalysts showed fairly stable polymerization kinetics. The catalyst activity, as a function of the silica calcination temperature, varied as follows: 250 °C > 600 °C > 800 °C > 450 °C. This finding has been explained considering the relevant surface chemistry phenomena. The calcination temperature did not significantly affect the bulk density and the PDI ($3.4 \leq \text{PDI} \leq 3.8$) of the resulting polyethylenes. The low PDI substantiates the retention of single-site catalytic behavior of the experimental supported catalysts.

Keywords: Supported zirconocene catalysts; Silica functionalization; Calcination temperature; Particle size distribution; Bulk density

1. Introduction

Silica is rated so far as the best support for heterogenizing metallocenes. However, the as-received silica contains physisorbed water, surface hydroxyl groups, and siloxane functionality [1–8]. The hydroxyl groups appear in several forms: single (isolated), geminal, and hydrogen-bonded. The degree of calcination temperature varies the surface functionalities and their concentrations. The post-calcination concentration of especially the hydroxyl groups dictates the tethering of the catalyst precursors to be loaded. Therefore, the calcination (dehydroxylation) temperature affects the surface chemistry and performance of the final supported catalyst.

Among commercial metallocenes, (^{n}BuCp)$_2$ZrCl$_2$ has been widely used to polymerize ethylene [9–17]. However, a review of the literature shows that studies investigating the influence of silica calcination temperature on heterogenizing metallocenes, particularly (^{n}BuCp)$_2$ZrCl$_2$ for ethylene polymerization, is fairly limited. dos Santos et al. [11] heterogenized (^{n}BuCp)$_2$ZrCl$_2$ directly on silica (Grace 948) calcined at varying temperatures. They neither functionalized nor modified silica using a coupling agent and/or methyl aluminoxane (MAO). The ethylene polymerization activity of the resulting catalysts was determined in the presence of the separately fed

* Corresponding author. Tel.: +966 3 860 3898; fax: +966 3 860 4509.
E-mail address: matiq@kfupm.edu.sa (M. Atiqullah).

0926-860X/$ – see front matter © 2007 Elsevier B.V. All rights reserved.
doi:10.1016/j.apcata.2007.01.023

10 wt% MAO cocatalyst. Lee [18] also studied the influence of silica calcination temperature on the performance of (EtoMe$_2$Si–{CH$_2$}$_6$–Cp)$_2$ZrCl$_2$ supported on silica (Grace 948) by polymerizing ethylene using the MAO cocatalyst.

The above studies used MAO in high concentration (Al:Zr ∼ 3000) to produce the active zirconocenium cations (^{n}BuCp)$_2$ZrMe$^+$ and (EtoMe$_2$Si–{CH$_2$}$_6$–Cp)$_2$ZrMe$^+$. The resulting cations are stabilized by the [MAOCl]$^-$ anion through some weak electrostatic attraction [19–21]. Consequently, the supported metallocenes are apt to leach off the support, particularly in the presence of the MAO cocatalyst. Hence, the surface of the catalyst will practically change in situ and polymerization will occur in solution. All these are reflected by the fouling of the reactor and the production of very low bulk density resin. Also, the occurrence of competitive diffusion between ethylene and the separately fed MAO adds to the aliased factorial interactions. Therefore, ethylene polymerization, in presence of separately fed MAO cocatalyst, cannot appropriately evaluate the influence of the calcination temperature on the performance of a supported catalyst.

Other disadvantages concerning the use of MAO (as a separate cocatalyst in polymerization processes) include its gelling characteristic, variations in quality from one production batch to another, and fouling of the reactor. Therefore, ethylene polymerization without separately feeding the MAO cocatalyst is a much better approach to study the above-stated influence. Also, such a polymerization mode is industrially desirable to achieve better resin bulk density, decrease the production cost, and overcome the MAO-related problems [19,20,22,23]. Hence, the objectives of the present study are to investigate the influence of silica calcination temperature on (a) the activity of the catalyst [silica ES70–^{n}BuSnCl$_3$/MAO/(^{n}BuCp)$_2$ZrCl$_2$] by polymerizing ethylene without separately feeding the MAO cocatalyst and (b) evaluate henceforth the immobilization characteristics of the supported catalysts by assessing reactor performance (fouling and kinetic profile) and selected properties of the resulting polyethylenes such as particle size distribution, bulk density, and particulate morphology. To the best of our knowledge, such a study has not yet been reported in the literature. The supported catalyst was prepared following the order shown above. The post-calcined silica was functionalized using ^{n}BuSnCl$_3$ because this organotin compound has shown to act as a novel spacer agent [24–26]. An interesting feature of ^{n}BuSnCl$_3$ is that Sn, having multicoordination number, is capable of forming covalent, as well as coordinate-covalent bonds with an appropriate ligand [27–32].

2. Experimental

2.1. Materials

Silica ES70 (from Crosfield), having surface area of 300 m^2/g, an average pore volume of 1.6 ml/g, particle size of 35 μm, and an average pore size of 195 Å, was used as the support.

(^{n}BuCp)$_2$ZrCl$_2$ and MAO (30 wt% in toluene) were purchased from Chemtura. The following chemicals – HCl, HF, H_3BO_3, $Al(NO_3)_3$ stock solution in dilute HNO_3 (1.0 × 10^3 mg Al/l), ammoniumhexafluorosilicate $(NH_4)_2SiF_6$ (1.0 × 10^3 mg Si/l), $AlCl_3$, and $ZrCl_4$ stock solution (1.0 × 10^3 mg Zr/l) – used for determining the elemental composition of the synthesized catalysts, were obtained from BDH.

Analytical grade toluene and *n*-hexane (both 99.999% pure), molecular sieves, 0.05% (w/v) 2,6-di-*tert*-butyl-4-methyl phenol (BHT), and 1,2,4 trichlorobenzene (TCB)—all were obtained from Aldrich. ^{n}BuSnCl$_3$ was bought from Gellest Chemicals, USA. Acetylene, ethylene, hydrogen, and nitrous oxide (99.999% pure) were procured from Abdullah Hasim, a local vendor.

2.2. Determination of silica hydroxyl content

The hydroxyl content of the as-received and calcined silicas was determined using the apparatus (shown in Fig. 1) that consists of a high-precision electronic pressure transducer, a two-necked sample flask with a small dropping funnel, and an adapter having two outlets. Two separate valves, one of which is connected to the digital pressure transducer and the other to a vacuum manifold, operate these two outlets. The internal volume of the whole apparatus V_A was first determined by filling it with water.

A pre-weighed amount of silica was placed in the sample flask. The whole apparatus was assembled inside an inert atmosphere glove box. It was then connected to a vacuum manifold through valve V_1. About 10.0 ml of decahydronaphthalene (decalin) was added to the sample flask through the rubber septum of the dropping funnel by opening valve V_3. High vacuum was applied to the apparatus from the vacuum manifold by opening valves V_1–V_3. When the pressure transducer read zero, argon was fed into the apparatus through the vacuum manifold until a pressure of 1000 mbar was attained.

The above procedure was repeated thrice to remove air from the apparatus. Finally, the pressure in the apparatus was reduced to 500 mbar. Then valves V_1 and V_3 were closed. About 2.0 ml

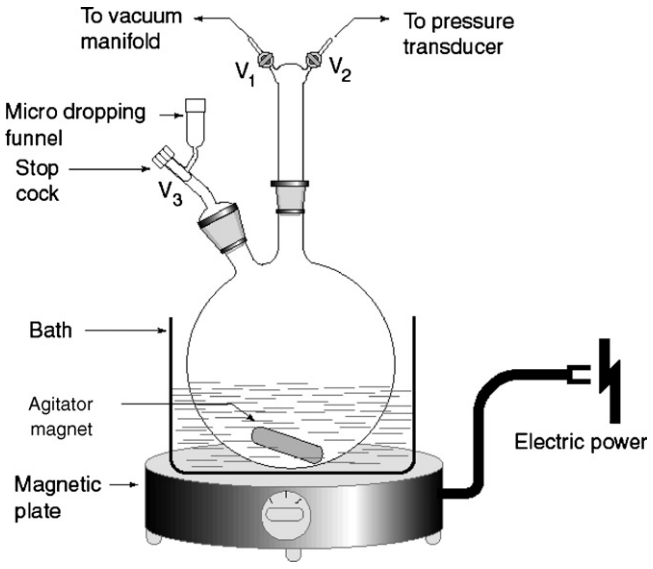

Fig. 1. Apparatus for determining silica hydroxyl groups.

of methylmagnesium iodide (MeMgI, a highly reactive Grignard reagent) was put into the dropping funnel using a syringe. The reading of the pressure transducer P_i was recorded. MeMgI was allowed to react, under vigorous magnetic stirring, with the silica in the sample flask by very slowly opening valve V_3. MeMgI reacted with the hydroxyl functionality of silica to produce methane, and increased the pressure that the transducer read. Upon completion of the reaction, the pressure transducer recorded the final reading P_f. The above operating conditions – the use of highly reactive MeMgI and a very high precision pressure transducer, as well as vigorous stirring of the reaction mass – were applied to ensure that MeMgI effectively and completely reacts with all the –OH functionality.

A blank titration that uses no silica was conducted by repeating the above procedure. P_b determined the pressure transducer reading corresponding to the blank titration. Finally, the silica hydroxyl content was determined using the following equation:

$$\frac{\text{mmol OH}}{\text{g silica}} = \frac{(P_f - P_i - P_b)\,(\text{mbar}) \times V_A\,(\text{l}) \times 10^3 (\text{mmol/mol})}{986.90\,(\text{mbar/atm}) \times 0.082058\,(\text{l atm/mol K}) \times \text{temp}\,(\text{K}) \times \text{silica}\,(\text{g})} \quad (1)$$

The accuracy of the hydroxyl content measured by the above MeMgI-based method was checked in two ways. First, the hydroxyl content of a given amount of β-naphthol was determined as described above. Then this value was compared with the stoichiometric one predicted by a complete reaction between β-naphthol and MeMgI. For example, the measured OH content for an experimental mass of β-naphthol was found to be 4.20 mmol against the stoichiometric one, 4.37 mmol.

Secondly, the measured hydroxyl content was compared with that determined by the thermogravimetric (TG) method [33–35]. Some representative comparative values are provided as follows. The hydroxyl content of the as-received silica PQ 3050 and that dehydroxylated at 110 °C for 4 h, determined by the MeMgI-based method, are 9.24 and 6.94 mmol/g silica, respectively while those by the TG-based method are 10.60 and 6.81 mmol/g silica, respectively.

We found using TG that most of the commercial silicas, including the one used in the present study, lose all the physisorbed water when they are heated at about 180 °C. Hence, the experimental silicas calcined at 250, 450, 600, and 800 °C for 4 h do not contain any residual water which is a potential source for interference with the measured values.

2.3. Catalyst synthesis

All the manipulations were done under an inert atmosphere of argon using standard Schlenk technique. The solvents used were dried using 4A type molecular sieve.

The required amount of silica was dehydroxylated at 250, 450, 600, and 800 °C for 4 h using a Thermcraft furnace equipped with a vertical quartz glass tube, a digital temperature indicator and controller, a gas flow meter, and a vacuum pump. The silica was continuously fluidized using nitrogen. Upon dehydroxylation, it was stored in an inert glove box.

The dehydroxylated silica was functionalized using ^{n}BuSnCl$_3$ as follows. The required amount of silica was placed in a 250 ml Schlenk flask under argon. Then it was slurried with 70.0 ml of dry toluene under continuous magnetic stirring; 1.30 g of ^{n}BuSnCl$_3$ was injected into the silica–toluene slurry. The resulting mixture was refluxed at 130 °C for 24 h. The final solid product was filtered, washed thrice with 30.0 ml of toluene, thrice with 20.0 ml of *n*-pentane, and dried for several hours under high vacuum. What follows summarizes the synthesis of the final catalyst.

The above-functionalized silica (3.0747 g) was placed in the catalyst synthesis reactor described in Ref. [21]. The functionalized silica was slurried by adding 20.0 ml of dry toluene to it. Then 9.8 ml of the as-received 30 wt% MAO was slowly added to the above slurry at room temperature and was continuously stirred for 60 min. Hence, the 30 wt% MAO makes an in situ component of the supported catalyst composition.

Next (^{n}BuCp)$_2$ZrCl$_2$ (0.2460 g) was separately placed in a Schlenk flask and was dissolved in 15.4 ml of dry toluene. This (^{n}BuCp)$_2$ZrCl$_2$ solution was injected into the reactor and was again stirred continuously for 60 min. Following this, the final catalyst was dried under high vacuum at 55 °C for several hours.

2.4. Catalyst characterization

2.4.1. Catalyst elemental composition

The bulk elemental compositions of the synthesized catalysts (in terms of Al, Si, Sn, and Zr) were determined by atomic absorption (AA) spectroscopy using the Perkin-Elmer equipment AAnalyst 100. The wavelengths of 309.3, 251.6, 235.5, and 360.1 nm represented Al, Si, Sn, and Zr, respectively [36]. High purity nitrous oxide-acetylene flame was used for the analyses. The determination of each element involved two common steps—calibration of the AA spectrometer and preparation of the experimental sample solution. The procedure for determining Al, Si, and Zr, are detailed elsewhere [21]. Therefore, what follows summarizes only the determination of Sn (tin).

The AA spectrometer was calibrated using spectrosol standard solution (1.0×10^3 mg Sn/l from BDH). The experimental sample solution was prepared as follows. About 50.0 mg of the catalyst sample was transferred to a 60 ml Teflon bottle having a tight seal cap. Half a milliliter of deionized water, 2.0 ml HF, and 1.0 ml HNO_3 were sequentially added to the catalyst sample. The bottle was tightly closed and heated in a water bath at 70 °C for 0.5 h. After this, the catalyst sample bottle was removed from the water bath and cooled to room temperature. The resulting solution was diluted to 50.0 ml by adding deionized water in a volumetric flask and was used for the analysis of tin.

Table 1 shows the elemental compositions of the synthesized catalysts.

Table 1
Elemental compositions of the synthesized catalysts

Catalyst code	Description	Calcination temperature (°C)	Composition (wt%)			Al:Zr molar ratio
			Sn	Zr	Al	
Catalyst 1	ES70–^{n}BuSnCl$_3$/MAO/(^{n}BuCp)$_2$ZrCl$_2$	250	0.08	0.74	18.5	84.50
Catalyst 2	ES70–^{n}BuSnCl$_3$/MAO/(^{n}BuCp)$_2$ZrCl$_2$	450	0.04	0.76	17.8	79.16
Catalyst 3	ES70–^{n}BuSnCl$_3$/MAO/(^{n}BuCp)$_2$ZrCl$_2$	600	0.04	0.68	19.6	97.42
Catalyst 4	ES70–^{n}BuSnCl$_3$/MAO/(^{n}BuCp)$_2$ZrCl$_2$	800	0.04	0.77	17.8	78.13

MAO = 30 wt% methylaluminoxane from Chemtura.

2.5. Polymerization trials

Ethylene was polymerized using a computer-interfaced, Imtech laboratory-scale reactor set up. The details are available elsewhere [21]. The 1-l glass reactor was baked for 1 h at about 120 °C. Then it was pressure-purged with nitrogen four to five times at about the same temperature. About 450 ml of hexane was transferred to the reactor. The resulting mixture was stirred at 50 rpm for 10 min.

The desired amount of the catalyst (30–40 mg as per the Zr loading) was placed in a 250 ml round bottom Schlenk flask in an inert atmosphere glove box. Then it was slurried in the Schlenk flask using 50.0 ml of hexane. One end of a Teflon tube provided with a swagelok nut was connected to the reactor feed port. The other end was dipped into the bottom of the catalyst slurry through a rubber septum closing the flask. The catalyst slurry was then transferred into the reactor (under positive pressure of argon) by opening the feed port valve. It was kept in suspension by swirling the flask, and the polymerization diluent (hexane) was stirred at about 100 rpm during this transfer process. After transfer of the catalyst slurry, the feed port valve was closed and the reactor was heated to 75 °C.

Feeding the reactor with ethylene to a total pressure of 8.5 bar(g) started the polymerization which was continued for 1 h at 400 rpm. Stopping the ethylene flow and venting the post-polymerization ethylene (in the reactor) to the atmosphere quenched the polymerization. Then, the data acquisition was stopped and the stirrer speed was reduced to about 100 rpm and the reactor was gradually cooled to the room temperature.

Upon completion of the polymerization trials as described above, the reactor was opened; the resulting polymer was filtered, dried under ambient conditions in a hood, and weighed.

2.6. Polymer characterization

The synthesized polyethylenes were characterized in terms of molecular weight distribution (polydispersity index) and average molecular weight using gel permeation chromatography (GPC). The GPC assay was done at 150 °C using Waters Alliance GPC 2000 model. Two mixed bed columns (PLgel 10 μm, Polymer Laboratories) were used.

The antioxidant, 0.05% (w/v) 2,6-di-*tert*-butyl-4-methyl phenol (BHT), was added to 1,2,4-trichlorobenzene (TCB) to prevent the polymer sample from degrading. A sample solution of 0.075–0.100% (w/v) was prepared at 150 °C in this antioxidant-containing solvent. The resulting solution (200 μl) was injected into the GPC column. The chromatogram data were acquired and analyzed using the Millenium[32] software.

The equipment was calibrated using polystyrene standards. The polystyrene-based calibration curve was converted into the universal one using the Mark–Houwink constants (values) of polystyrene ($K = 0.000121$ dl/g and $\alpha = 0.707$) and polyethylene ($K = 0.000406$ dl/g and $\alpha = 0.725$) [37].

2.7. Measurement of catalyst and resin particle size distribution

The particle size distribution of the catalyst and the polymer sample(s) was measured using the computer-interfaced Mastersizer 2000 particle size analyzer (Malvern Instruments, UK). This instrument works on the principle of laser diffraction. It is equipped with a 50–120 ml capacity Hydro 2000S liquid feeder which has a built-in ultrasound probe with an online pump and a stirrer.

A small amount of the catalyst sample (about 0.5 g) that shows an obscursion limit of ~5.0% was dispersed in de-ionized water. However, for the polymeric sample, a few drops of surfactant were added to the water to help dispersion. The optical properties of the samples were selected from the library of materials available in the provided software. Each sample was analyzed using five cycles having various stirrer speeds and different intensities of ultrasound. The particle size distribution and its average were calculated using Mie theory.

2.8. Measurement of catalyst and resin particulate surface morphology

The catalyst and the experimental polyethylene samples were first coated with a layer of carbon to increase the surface conductivity. These coated samples were characterized using a scanning electron microscope (SEM) equipped with an energy dispersive X-ray spectrometer (EDS). The particulate morphology was evaluated by operating the electron microscope in the backscattered electron imaging (BEI) mode.

2.9. Measurement of resin bulk density

The bulk density of the experimental polyethylenes was determined using the Apparent Density Tester (Model No. 1132, manufactured by IPT, Germany) according to ISO 60 [38].

3. Results and discussion

First, the performance of ethylene polymerization without separately feeding the MAO cocatalyst, in terms of reactor operability, resin particulate morphology, and polymerization kinetics, is discussed. However, recall in this context that the experimental catalyst loads 30 wt% MAO (not the 10 wt% analogue); and the structure and constituent of MAO vary with its solution concentration. For example, the total aluminum content, aluminum containing free and associated trimethyl aluminum (TMA), aluminum belonging to free and associated TMA relative to total aluminum, and methyl to aluminum ratio of 30 wt% MAO differ from those of the 10 wt% analogue [39].

Here we evaluate the immobilization characteristics of the synthesized supported catalysts under the experimental conditions through assessment of reactor performance and product morphology. No reactor fouling was observed. Free-flowing polymer particles were obtained. Fig. 2 compares the particle size distribution (PSD) of Catalyst 1 with that of the resulting polyethylene whereas Table 2 lists the statistical parameters of the corresponding distributions. Fig. 2 shows that the original catalyst particles fragmented during polymerization and polymer grew around these fragments increasing the resin particle size. It also demonstrates that the PSD of the polymer resembles that of the catalyst. These findings confirm the occurrence of the replication phenomenon from the catalyst to the polymer. The PSD span of the product is 1.41, which is fairly narrow (Table 2). This value falls within the range that is required for various mixing-intensive polymer applications [40–43]. Hence, the merits of the present catalyst system and the polymerization of ethylene without separately feeding the MAO cocatalyst are further established.

Figs. 3 and 4 show the SEM photographs of Catalyst 1 and the corresponding polyethylene resins produced, respectively. The resin particles are of about spherical morphology similar to that of the catalyst particles. Fig. 5 shows stable polymerization kinetics.

The above results substantiate that ethylene polymerization without separately feeding the MAO cocatalyst prevents leaching and favors heterogeneous catalysis to occur. In the absence of MAO (the leaching aid), the polymer film formed instantaneously around a catalyst particle coats/immobilizes the catalyst constituents; this is how leaching is in situ prevented. This is somewhat similar to the conventional pre-polymerization that is done with supported olefin polymerization catalysts. The work of

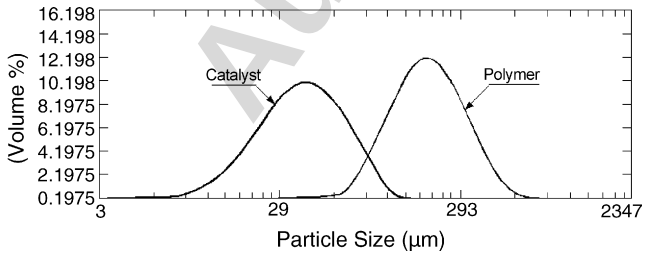

Fig. 2. Particle size distribution of Catalyst 1 and that of the resulting polymer. Other catalysts show similar behavior; to avoid duplication they are not reported.

Table 2
Statistical parameters of the particle size distribution of Catalyst 1 and the resulting polyethylene resin

Sample code	Volume-weighted mean (μm)	$d(0.1)$ (μm)	$d(0.5)$ (μm)	$d(0.9)$ (μm)	PSD span[a]
Catalyst 1	40.56	12.65	36.83	74.05	1.68
Polyethylene resin	235.62	98.04	192.40	369.92	1.41

$d(0.1)$, $d(0.5)$, and $d(0.9)$ mean that 10%, 50%, and 90% of the particles have less than or equal to the corresponding indicated particle diameter (μm), respectively. Other catalysts show similar behavior; to avoid duplication they are not reported. PSD: particle size distribution.

[a] $[d(0.9) - d(0.1)]/d(0.5)$.

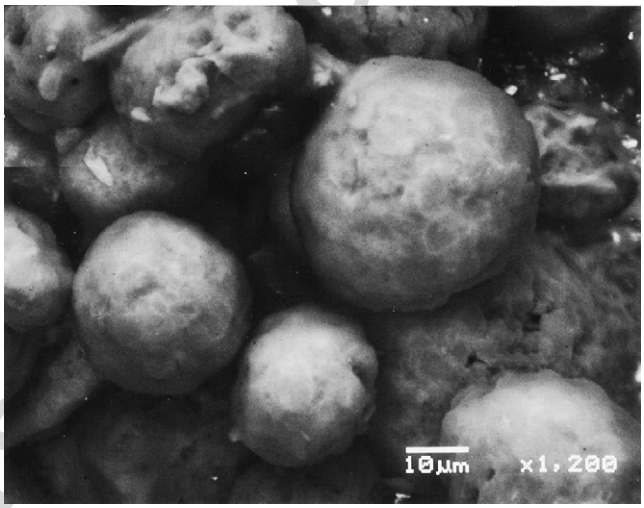

Fig. 3. SEM picture of Catalyst 1.

Smit et al. [44,45], whose catalyst synthesis procedure fairly matches that of ours, as well supports this remark. They also polymerized ethylene without separately feeding the MAO cocatalyst. They confirmed by taking the scanning electron microscopic (SEM) cross-sectional photograph of time-dependent polyethylene particles that the polymer grew on the catalyst

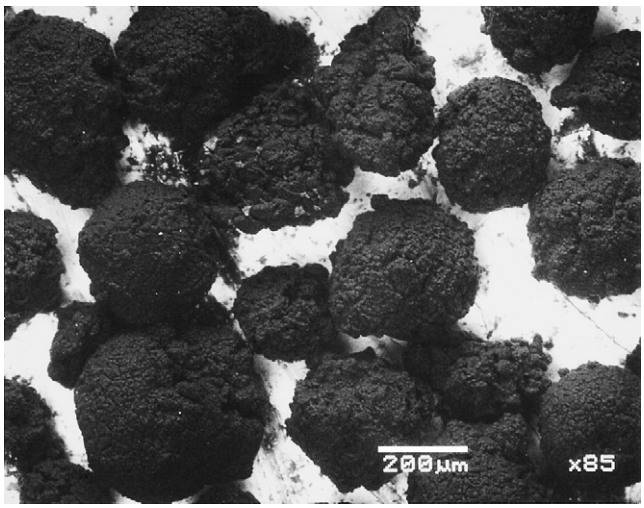

Fig. 4. SEM picture of the resin particle(s) produced by Catalyst 1.

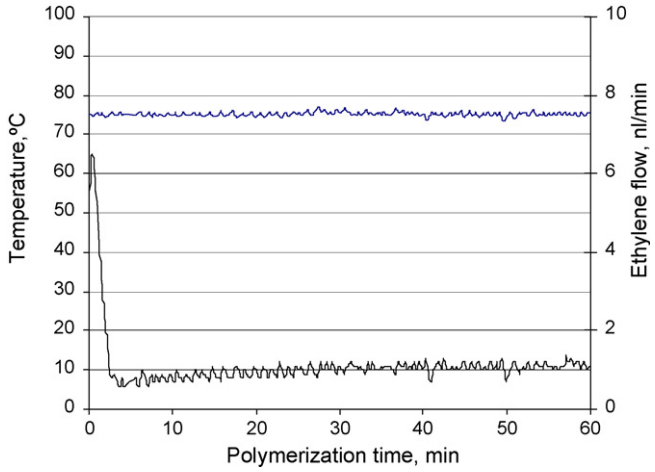

Fig. 5. Kinetic profile of Catalyst 1. The top curve relates to temperature while the bottom one to ethylene flow rate. Polymerization trials were conducted without separately feeding the MAO cocatalyst. Polymerization conditions: pressure = 8.5 bar(g); temperature = 75.0 °C; time = 1 h. Other catalysts show similar behavior; to avoid duplication they are not reported.

particles; polymerization did not occur in the solution phase. Note that Smit et al. did not use any coupling agent in catalyst synthesis. Also, their objectives differ from those of the present study.

Next, the influence of silica calcination temperature on the overall performance of the synthesized supported catalysts, in context of the present theme, is discussed.

Fig. 6 ranks the catalyst activity as a function of the silica calcination temperatures as follows: 250 °C > 600 °C > 800 °C > 450 °C.The above was found even though the increasing calcination temperature continuously decreased the hydroxyl content on the silica surface (see Fig. 7). The coefficient of determination R^2 in Fig. 7 is 0.9975, which is very close to unity. The hydroxyl content of the experimental silica at higher temperatures is comparable with those of a number of silicas reported in the literature [46]. Fig. 8 shows how this decreasing hydroxyl content affected the loading of $BuSnCl_3$. A temperature of 250 °C loaded the maximum tin on the dehydroxylated silica; then, the tin loading dropped up to about 600 °C. Beyond this calcination temperature, the tin loading increased. However, the

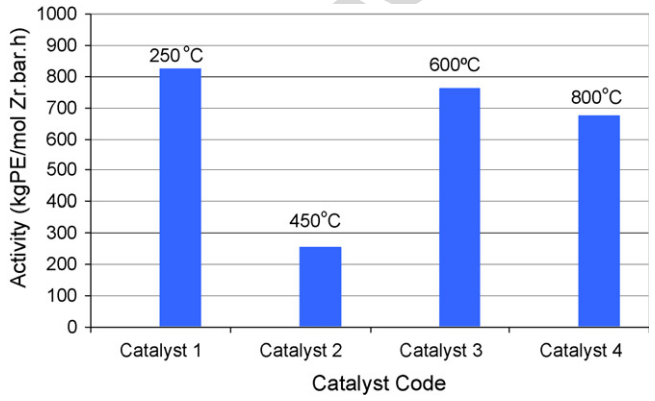

Fig. 6. Effect of silica calcination temperature on the catalytic activity of ethylene polymerization without separately feeding the MAO cocatalyst. Polymerization conditions: pressure = 8.5 bar(g); temperature = 75.0 °C; time = 1 h.

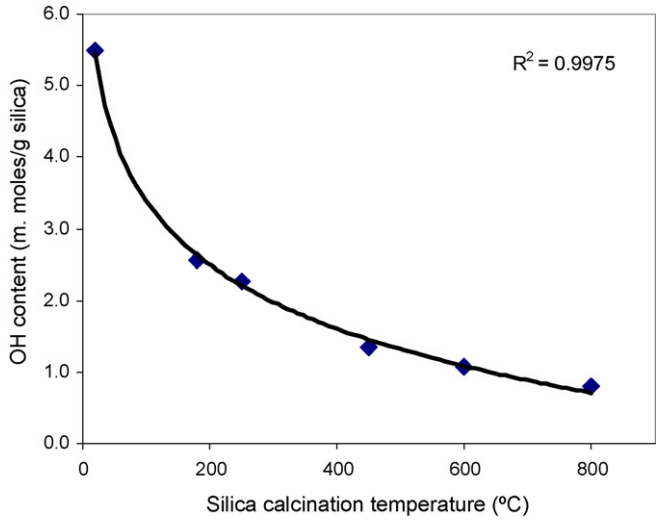

Fig. 7. Effect of calcination/dehydroxylation temperature on the hydroxyl content of silica ES70.

final catalysts did not reflect significant variation of the Sn and Zr content. Also, the Al:Zr molar ratio in each catalyst fairly remained the same (Table 1). These findings are explained below.

Between 250 and 600 °C, the tin loading is preferentially dictated by the formation of covalent bond through the reaction of the–OH functionality of silica with the Cl ligand of $^{n}BuSnCl_3$. A substitution reaction occurs between H of the –OH functionality and the Cl ligand, producing HCl. The hydroxyl content at 250 °C (2.27 mmol/g silica) decreased by 40.5, 52.9, and 63.3% at 450, 600, and 800 °C, respectively. With the increase in calcination temperature as stated above, the decreasing –OH content, therefore, reduced the loading of $^{n}BuSnCl_3$ on silica. However, beyond 600 °C, the reverse was noted despite the –OH content continued to drop as the calcination temperature was further elevated. The latter finding, which took place corresponding to about 50% decrease in hydroxyl content (with respect to that at 250 °C), may be explained as follows.

The –OH groups (geminal and/or isolated) convert/condense into the tricyclic (three-membered) siloxane

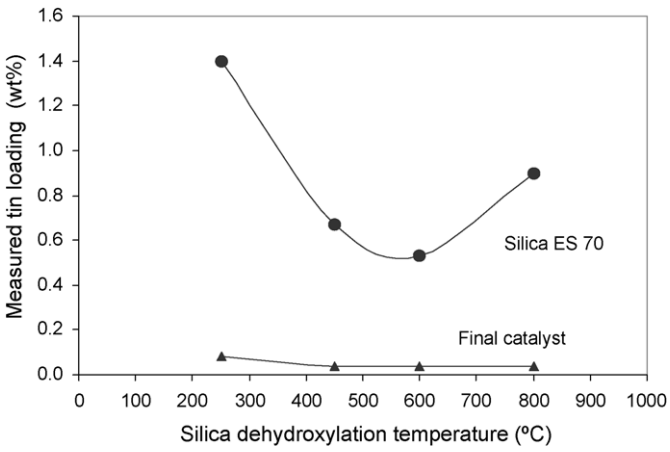

Fig. 8. Effect of calcination/dehydroxylation temperature on tin loading on silica ES70 and the final catalysts (Catalysts 1–4).

functionality – Si–Ö–Si – as a result of calcination. Hence, the gradual growth of siloxane functionality compensates for the loss of the –OH groups. This means that the concentration of the siloxane functionality increased with the increasing calcination temperature [5,6,8,18,47–50]. Above 600 °C, $^{n}BuSnCl_3$ predominantly got anchored to the siloxane functionality through the formation of a coordinate-covalent bond between the coordinately unsaturated Sn and the lone pair of Ö atom of the siloxane (which acted as the coordinating ligand). Sn can assume multi-coordination number. Hence, the resultant product is likely to be a multicoordinate organotin adduct. The relevant works published in the literature support this proposed bond formation and the corresponding product type [27–32]. Therefore, the increasing siloxane content increased the tin loading at a temperature above 600 °C. However, the observed drop of tin content in the final catalyst can be attributed to the gain in weight that resulted from the loading of MAO and $(^{n}BuCp)_2ZrCl_2$.

Now we address the situation concerning the tin loading in the final catalyst. Here, the loading of Zr and Al is, for example, about 9–19- and 231–445-fold that of tin, respectively. Also, the major mass is accounted for by that of silica. Consequently, the variation of tin content, within the experimental accuracy of atomic absorption spectroscopy, remained fairly unaffected.

The activity behavior of catalyst ES 70–$BuSnCl_3$/MAO/$(^{n}BuCp)_2ZrCl_2$ with respect to the calcination temperature is divided into two (Fig. 6). From 250 to 450 °C, the activity dropped. From 450 to 800 °C, the opposite occurred. This is explained below with reference to Schemes 1 and 2. These schemes have been drawn using Ref. [21] plus the works cited therein, and Refs. [27–32].

Scheme 1 illustrates how the catalyst will deactivate through the formation of the inactive bidentate zirconocene in absence of functionalization of silica by $^{n}BuSnCl_3$ and subsequent loading of MAO. Note that the bidentate zirconocene, being devoid of the labile extractable Cl^- ligand, will not generate the active metallocenium cation. Scheme 2 summarizes the surface chemistry that stepwise leads to the generation of the active metallocenium cation. Scheme 2a and b also show the anchoring of $^{n}BuSnCl_3$ to the dehydroxylated silica by covalent and coordinate-covalent bonds, respectively. The [supported-MAOCl]$^-$ polyanion pairs with and stabilizes the active $[(^{n}BuCp)_2ZrMe]^+$ cation. These schemes show that the variational loading of $^{n}BuSnCl_3$ will correspondingly influence the following factors – the minimization of steric hindrance, the prevention of bimolecular deactivation, the facile lability of the afore-said supported polyanion, and the generation of the active $[(^{n}BuCp)_2ZrMe]^+$ cation – which combinedly determine the catalytic activity. Note that the loading of $^{n}BuSnCl_3$ and the catalytic activity, as a function of the calcination temperature, vary in a fairly similar fashion. This explains the variation of activity as a function of the calcination temperature that Fig. 6 shows.

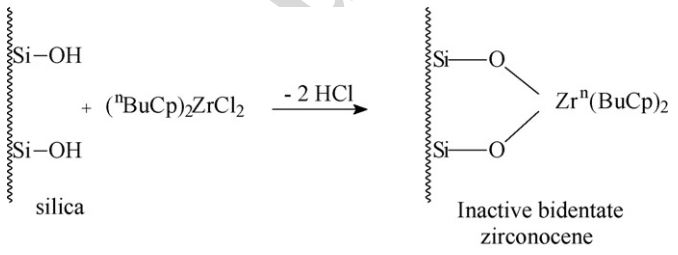

Scheme 1. Formation of the inactive bidentate zirconocene in absence of functionalization of silica by $^{n}BuSnCl_3$ and subsequent loading of MAO. See Ref. [21] for details.

What follows compares the above findings with that of dos Santos et al. [11] and Lee [18] who also investigated the influence of silica calcination temperature on the ethylene polymerization activity of selected supported metallocene catalysts. However, the present study differs from these published works summarized in Table 3. A major point of difference is that no MAO was separately fed as a cocatalyst; the 30 wt% MAO only forms an in situ component of the overall supported catalyst composition. Consequently, the

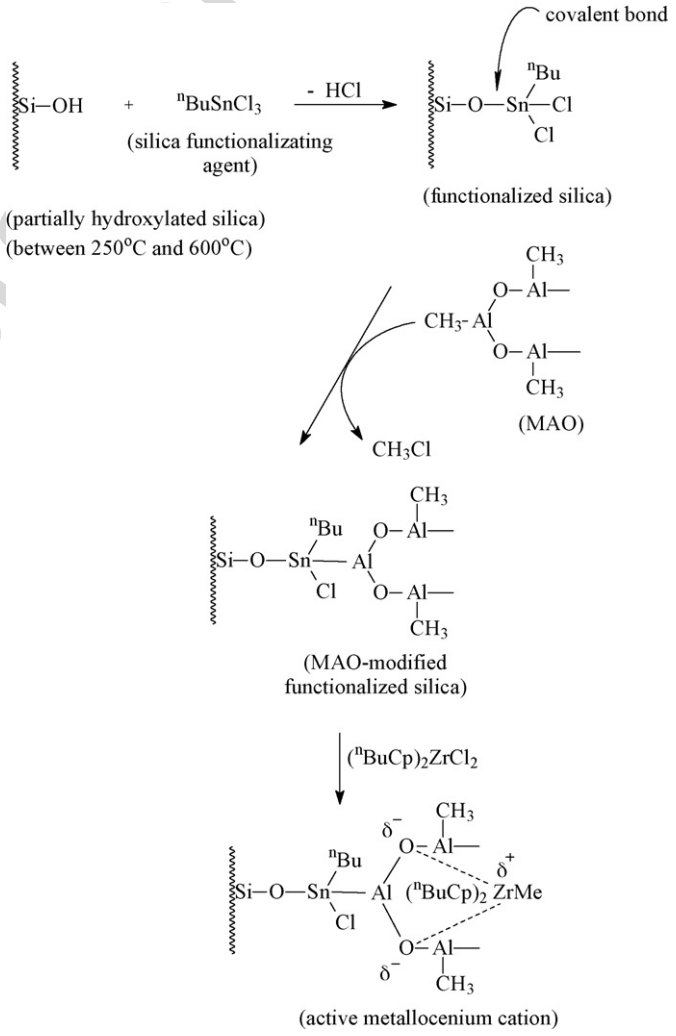

Scheme 2. (a) Surface chemistry of the supported catalyst silica ES70–^{n}-$BuSnCl_3$/MAO/$(^{n}BuCp)_2ZrCl_2$) at ≤600 °C. This has been drawn following Ref. [21] and the relevant literature cited therein. (b) Surface chemistry of the supported catalyst silica ES70–$^{n}BuSnCl_3$/MAO/$(^{n}BuCp)_2ZrCl_2$) at ≥500 °C. This has been drawn following Ref. [21] plus the relevant literature cited therein, and Refs. [27–32].

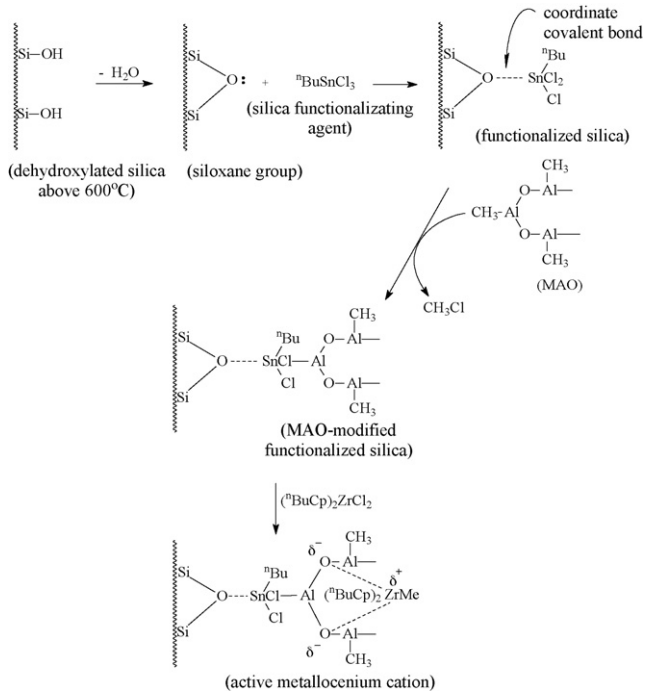

Scheme 2 (*Continued*).

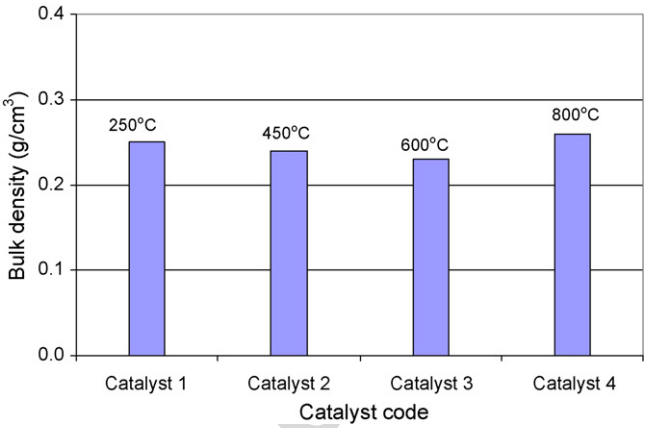

Fig. 9. Effect of silica calcination/dehydroxylation temperature on the bulk density of the polyethylenes resulting from polymerization without separately feeding the MAO cocatalyst. Polymerization conditions: pressure = 8.5 bar(g); temperature = 75.0 °C; time = 1 h.

experimental slurry polymerization trials are not affected by the competitive diffusion of ethylene and MAO. Opposite is the case when MAO feeds the reactor as a cocatalyst.

The catalyst performance, despite the above variations, can be assessed as follows:

(i) A common phenomenon was observed between the present study catalysts and those of dos Santos et al. [11]. With the increasing calcination temperature, the catalyst activity first decreased, then it increased. In the present study, the maximum decrease in activity corresponds to 450 °C while the work of dos Santos et al. shows this to occur at 207 °C.

(ii) The Lee [18] catalyst activity, unlike the above, continuously increased as the silica calcination temperature was increased from 200 to 800 °C. This increase in calcination temperature, however, continuously decreased the silica hydroxyl content without significantly affecting the zirconium loading. Competitive anchoring of the metallocene with the hydroxyl versus siloxane groups was ascribed to this finding.

In our investigation, the increasing calcination temperature did not significantly affect the bulk density of the resulting polyethylenes (see Fig. 9); 0.23 g/ml $\leq$ bulk density $\leq$ 0.27 g/ml.

The effect of calcination temperature on the weight average molecular weight M_w was as follows. The temperature (450 °C), corresponding to which minimum activity was found, showed the maximum M_w (see Fig. 10). This can be attributed to the decrease in the rates of polymer chain propagation (growth) and chain termination such that the decrease in the former is less than the decrease in the latter so that resultantly the ratio of the rates of chain propagation to chain termination corresponding to the calcination temperature of 450 °C is higher than that concerning the remaining calcination temperatures. An inverse relation between activity and M_w has also been reported elsewhere in the literature [18,51–53]. In the present study, the PDI remained hardly unaffected; $3.4 \leq \text{PDI} \leq 3.8$ (see Fig. 11), showing the retention of single-site catalytic behavior in the solid-state, and the paired and stabilized metallocenium cations shown in Scheme 2a and b are essentially the same.

Table 3
Silica calcination temperatures vs. ethylene polymerization conditions published in the literature [11,18]

Polymerization parameters	Present study	dos Santos et al. [11]	Lee [18]
Calcination temperature (°C)	250, 450, 600, 800	100, 207, 315, 450	200, 400, 600, 800
Catalyst system	ES70–^{n}BuSnCl$_3$/MAO[a]/(^{n}BuCp)$_2$ZrCl$_2$	Grace 948/(^{n}BuCp)$_2$ZrCl$_2$	Grace 948/[(Eto)Me$_2$Si–(CH$_2$)$_6$Cp]$_2$ZrCl$_2$
Polymerization diluent	Hexane	Toluene	Hexane
Pressure (bar)	8.5	1.0	2.7
Temperature (°C)	75.0	70.0	80.0
Time (min)	60	30	60
Cocatalyst	No MAO was separately fed as a cocatalyst	10 wt% Chemtura MAO was fed as a cocatalyst	6 wt% Akzo Nobel MMAO was fed as a cocatalyst
Al:Zr molar ratio	78–97 (in the catalyst)	3000	Not reported

[a] 30 wt% methylaluminoxane from Chemtura.

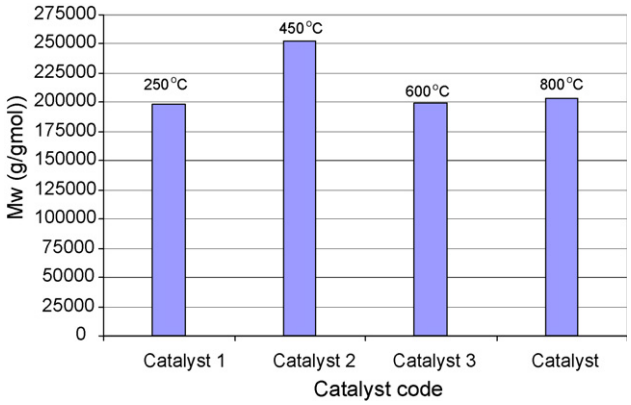

Fig. 10. Effect of silica calcination/dehydroxylation temperature on the weight average molecular weight of the polyethylenes resulting from polymerization without separately feeding the MAO cocatalyst. Polymerization conditions: pressure = 8.5 bar(g); temperature = 75.0 °C; time = 1 h.

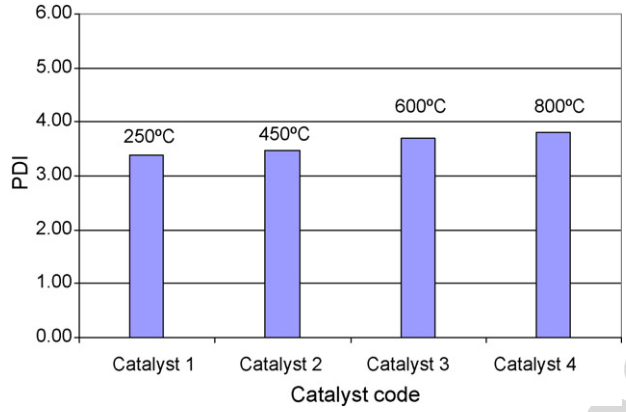

Fig. 11. Effect of silica calcination/dehydroxylation temperature on the polydispersity index (PDI) of the polyethylenes resulting from polymerization without separately feeding the MAO cocatalyst. Polymerization conditions: pressure = 8.5 bar(g); temperature = 75.0 °C; time = 1 h.

4. Conclusions

The present study on ethylene polymerization in absence of the separately fed MAO cocatalyst concludes the following:

1. No reactor fouling was observed. Free-flowing polymer particles, with a spherical morphology similar to that of the catalyst particles, were obtained. The particle size distribution of the polymer resembled that of the catalyst. Therefore, the replication phenomenon from catalyst to polymer took place.
2. Ethylene polymerization, in absence of the separately fed MAO cocatalyst, formed a polymer film around the catalyst particle, which coated/immobilized the catalyst constituents; this is how leaching was in situ prevented which favored heterogeneous catalysis to occur. The formation of free-flowing polymer particles with good bulk density reflects what has been stated above.
3. The product that resulted from ethylene polymerization without separately feeding the MAO cocatalyst showed a PSD span of 1.41. This value falls well within the range that is desired for various mixing-intensive polymer applications.
4. The catalysts showed fairly stable polymerization kinetics.
5. The catalyst activity as a function of the silica calcination temperatures varied as follows: 250 °C > 600 °C > 800 °C > 450 °C.

   This shows that from 250 to 450 °C, the activity dropped whereas from 450 to 800 °C, the opposite occurred. This happened even though the increasing calcination temperature continued to decrease the hydroxyl content on the silica surface.
6. The increasing calcination temperature did not significantly affect the bulk density of the resulting polyethylenes (0.23 g/ml ≤ bulk density ≤ 0.27 g/ml) and the PDI (3.4 ≤ PDI ≤ 3.8). The narrow PDI substantiates the retention of single-site catalytic behavior of the experimental supported catalysts.
7. The calcination temperature offering the minimum activity, that is, 450 °C showed the maximum M_w.
8. This work will help future metallocene heterogenization studies that are likely to use silica functionalizing agents capable of forming covalent as well as coordinate-covalent bonds.

Acknowledgements

The authors thankfully acknowledge the support provided by the Research Institute and the Department of Chemistry of King Fahd University of Petroleum & Minerals, Dhahran, Saudi Arabia for the present study. The industrial collaboration and fund provided by Saudi Basic Industries Corporation (SABIC), under Project No. 21164, are especially acknowledged. The technical assistance of Messrs Neaz Ahmed and Khurshid Alam is also highly acknowledged. The authors greatly appreciate the constructive comments of the reviewers.

References

[1] P. Hoffmann, E. Knozinger, Surf. Sci. 188 (1987) 181.
[2] B.C. Bunker, D.M. Haaland, T.A. Michalske, W.L. Smith, Surf. Sci. 222 (1989) 95.
[3] T.E. Nowlin, R.I. Mink, F.Y. Lo, T. Kumar, J. Polym. Sci. A: Polym. Chem. 29 (1991) 1167.
[4] C. Louis, M. Che, J. Catal. 135 (1992) 156.
[5] S. Haukka, E.L. Lakomaa, A. Root, J. Phys. Chem. 97 (1993) 5085.
[6] S. Haukka, E.-L. Lakomaa, O. Jylha, J. Vilhunen, S. Hornytzkyj, Langmuir 9 (1993) 3497.
[7] S.K. Ihm, K.J. Chu, J.H. Yim, in: K. Soga, M. Terano (Eds.), Catalyst Design for Tailor-made Polyolefins: Studies in Surface Science, Elsevier, New York, 1994, pp. 299–306.
[8] E.I. Iiskola, S. Timonen, T.T. Pakkanen, O. Härkki, P. Lehmus, J.V. Seppälä, Macromolecules 30 (1997) 2853.
[9] M. Chang, European Patent 323 716 A1 (1989), to Exxon Chemical Patents.
[10] G.B. Galland, M. Seferin, R.S. Mauler, J.H.Z. dos Santos, Polym. Int. 48 (1999) 660.
[11] J.H.Z. dos Santos, C. Krug, M.B. da Rosa, F.C. Stedile, J. Dupont, M.C. Forte, J. Mol. Catal. A: Chem. 139 (1999) 199.
[12] A. Andersen, R. Blom, I.M. Dahl, Macromol. Chem. Phys. 202 (2001) 726.

[13] P. Kumkaew, L. Wu, P. Praserthdam, S.E. Wanke, Polymer 44 (2003) 4791.
[14] H.P. Dornik, G. Luft, A. Rau, T. Wieczorek, Macromol. Mater. Eng. 288 (2003) 558.
[15] K.B. Yoon, Macromol. Res. 12 (2004) 336.
[16] L. Wu, J.-M. Zhou, D.T. Lynch, S.E. Wanke, Appl. Catal. A: Gen. 293 (2005) 180.
[17] K.-B. Yoon, D.-H. Lee, S.K. Noh, Macromol. Res. 14 (2006) 240.
[18] B.-Y. Lee, WIPO Patent WO 99 52949 (1999), to LG Chemical Ltd.
[19] S.J. Lancaster, S.M. O'Hara, M. Bochman, in: W. Kaminsky (Ed.), Metalorganic Catalysts for Synthesis and Polymerization, Springer, New York, 1999, pp. 413–425.
[20] S. Charoenchaidet, S. Chavadej, E. Gulari, J. Mol. Catal. A: Chem. 185 (2002) 167.
[21] M. Atiqullah, M.N. Akhtar, M. Faiz, A. Moman, A.H. Abu-Raqabah, J.H. Khan, M.I. Wazeer, Surf. Interf. Anal. 38 (2006) 1319.
[22] Y. Nakayama, H. Bando, Y. Sonobe, T. Fujita, Bull. Chem. Soc. Jpn. 77 (2004) 617.
[23] J.R. Severn, J.C. Chadwick, Macromol. Rapid Commun. 25 (2004) 1024.
[24] M. Atiqullah, A. Moman, M.N. Akhtar, A.R. Atieh, S.J. Palackal, M.A. Al-Saleh, F. Rahman, M. Ibrahim, J.H. Khan. WO Patent 2004094480 A2 (2004), to Saudi Basic Industries Corporation.
[25] M. Atiqullah, A. Moman, M.N. Akhtar, A.R. Atieh, S.J. Palackal, M.A. Al-Saleh, F. Rahman, M. Ibrahim, J.H. Khan, US Patent 6 908 876 B2 (2005), to Saudi Basic Industries Corporation.
[26] M. Atiqullah, A. Moman, M.N. Akhtar, A.R. Atieh, S.J. Palackal, M.A. Al-Saleh, F. Rahman, M. Ibrahim, J.H. Khan. EP Patent 1613667 A2 (2006), to Saudi Basic Industries Corporation.
[27] J.N. Spencer, B.G. Enders, A. Grushow, S.P. Kneizys, W.L. Nachlis, D. Mokrynka, S.M. Coley, C. Otter, C.H. Yoder, J. Organomet. Chem. 362 (1989) 53.
[28] S. Dostal, S.J. Stoudt, P. Fanwick, W.F. Sereatan, B. Kahr, J.E. Jackson, Organometallics 12 (1993) 2284.
[29] K.F.E. Williams, C.E. Johnson, J.A. Johnson, D. Holland, M.M. Karim, J. Phys.: Condens. Matter 7 (1995) 9485.
[30] C.H. Yoder, L.A. Margolis, J.M. Horne, J. Organomet. Chem. 633 (2001) 33.
[31] N.C. Lloyd, B.K. Nicholson, A.L. Wilkins, R. Thomson, Chem. N.Z. 66 (2002) 53.
[32] A.A. Kudrinsky, P.G. Mingalyov, A.V. Fionov, G.V. Lisichkin, Russ. Chem. Bull. 54 (2005) 146.
[33] J.J. Fripiat, J. Uytterhoeven, J. Phys. Chem. 66 (1962) 800.
[34] S. Ek, A. Root, M. Peussa, L. Niinisto, Thermochim. Acta 379 (2001) 201.
[35] R. Mueller, H.K. Kammler, K. Wegner, S.E. Pratsinis, Langmuir 19 (2003) 160.
[36] Perkin-Elmer, Atomic Absorption Spectroscopy: Analytical Methods, Manual No. 0303-1052, Release D. The Perkin-Elmer Corporation, Norwalk, CT, 1996.
[37] L.I. Kulin, N.L. Meijerink, P. Starck, Pure Appl. Chem. 60 (1988) 1403.
[38] F.N. Cogswell, Polymer Melt Rheology: A Guide for Industrial Practice, Geogre Godwin/John Wiley, New York, 1981.
[39] W.R. Beard, D.R. Blevins, D.W. Imhoff, B. Kneale, L.S. Simeral, Presented in Polyethylene—New Technology, New Markets. Organized by the Institute of Materials, London, UK, October 24, 1997.
[40] B.E. Wagner, A.V. Ramamurthy, EP 713888 A2 (1996), to Union Carbide Chemicals & Plastics Technology Corporation, USA.
[41] H. Murakami, J. Yoshizono, M. Kioka, JP 11302289 A2 (1999), to Mitsui Chemicals Inc., Japan.
[42] A.V. Ramamurthy, C.C. Williams, US 6 150 478 A (2000), to Union Carbide Chemicals & Plastics Technology Corp., USA.
[43] S. Huchette, P. Leaney, F.R.M.M. Morterol, WO 2003044064 A1 (2003), to BP Chemicals Ltd., UK.
[44] M. Smit, X. Zheng, J. Loos, J.C. Chadwick, C.E. Koning, J. Polym. Sci. A: Polym. Chem. 43 (2005) 2734.
[45] M. Smit, X. Zheng, R. Brüll, J. Loos, J.C. Chadwick, C.E. Koning, J. Polym. Sci. A: Polym. Chem. 44 (2006) 2883.
[46] C. Sun, W. Liu, Z. Jing, W. Chen, Shiyou Lianzhi Yu Huagong 34 (2003) 5.
[47] E.A. Wovchko, J.C. Camp, J.A. Glass Jr., J.T. Yates Jr., Langmuir 11 (1995) 2592.
[48] C.J. Brinker, R.K. Brow, D.R. Tallant, R.J. Kirkpatrick, J. Non-Crystal. Sol. 120 (1990) 126.
[49] R.L. White, A. Nair, Appl. Spectrosc. 44 (1990) 69.
[50] L. Wang, Y.L. Yuan, C.X. Ge, Y.X. Wang, B. Ji, J. Pan, Z.Y. Ye, L.X. Feng, J. Appl. Polym. Sci. 76 (2000) 1583.
[51] J.C.W. Chien, B.P. Wang, J. Polym. Sci. A: Polym. Chem. 26 (1988) 3089.
[52] J.C.W. Chien, B.P. Wang, J. Polym. Sci. A: Polym. Chem. 28 (1990) 15.
[53] H.C. Welborn, C.S. Speed, EP 0260999 (1988), to Exxon Chemical Patents Incorporated, USA.